Microscopic Origins of Catastrophic Optical Damage in Diode Lasers

Martin Hempel, Jens W. Tomm, Fabio La Mattina, Ingmar Ratschinski, Martin Schade, Ivan Shorubalko, Michael Stiefel, Hartmut S. Leipner, Frank M. Kießling, and Thomas Elsaesser

***Abstract*—Extremely early phases of the catastrophic optical damage (COD) process in 808-nm emitting GaAs/$Al_{0.35}Ga_{0.65}As$ high-power diode lasers are prepared by the application of short single current pulses. Typical energy entries during these pulses are on the order of 100 nJ within several 100 ns. The resulting defect pattern is investigated by high-resolution microscopy. The root of the COD is found to be located at the waveguide of the laser structure. Analysis of material composition modifications as a result of early COD phase points to melting being involved in the process. During recrystallization, an Al-rich pattern is formed that encloses a volume of a few cube micron of severely damaged material.**

***Index Terms*—Semiconductor device measurements, semiconductor diodes, semiconductor lasers.**

I. Introduction

High-power diode lasers are the main source of photonic energy in a large variety of laser systems. Conversion efficiencies exceeding 70% make them the most efficient man-made tool for converting electric into photonic energy. This unique status calls for exploiting reserves that have not been fully used so far. Beyond the principal physical limits related to carrier capture and gain saturation, thermal effects still matter. This involves reversible effects such as the deterioration of beam properties but also irreversible processes such as degradation. The catastrophic optical damage (COD) process [1] [2] represents one important example for a sudden degradation process, which becomes of particular relevance at very high emission powers. Since this process typically causes a damage pattern starting at the outcoupling facet or in the interior of the device, it is rather straightforward to analyze this pattern in order to learn more about root-causes and the sequence of events of the process [3]–[11]. In this paper, we follow this strategy, but make one important distinction: We provoke the COD artificially under conditions, where we know, how much energy is introduced into the facet region in order to create the damage pattern. This allows us to reduce this energy with the goal to prepare extremely early stages of the process. As a result, we have available a new quality of degraded devices for microscopic investigations.

This paper is organized as follows; we start with an introduction of the laser structure and give the details on selective provocation of COD and generation of earliest phases of defect propagation. After a description of the microscopy equipment, we present the results of defect analysis in conjunction with the energy available to generate them. Thereafter, we discuss these facts from an overarching point of view. Waveguide layers are revealed as starting points of the COD process. Different physical mechanisms are identified for COD at the facet and in the interior of the cavity.

II. Experimental Details

A. Device Structures and Test Strategy

The devices are commercial 808-nm emitting broad-area GaAs/$Al_{0.35}Ga_{0.65}As$ diode lasers [12]. The gain-guided lasers have a length of 1.4 mm and an emitter stripe width of 50 μm. They are mounted p-down, i.e., with the epitaxial layer close to the copper heat sink. The scheme of a mounted device is shown in Fig. 1(a); the inset gives the epitaxial layer sequence. The coordinate system used throughout the entire report is indicated. The active medium is a $\sim$10-nm thick AlGaAs/GaAs quantum well (QW). Front and rear facets are coated with low ($\sim$3%) and high ($\sim$95%) reflectivity dielectric layers, respectively. The devices are designed for continuous wave (cw) operation at 0.6 A with an optical output power of (0.52 ± 0.01) W and a threshold current of (0.21 ± 0.01) A. The COD in these devices is provoked by using short single current pulses. It has been shown, at least for broad-area lasers, that this approach is suitable to generate the same type of damage pattern as observed for COD in long-term cw aging experiments [13]. Thus, this approach represents a special type of *accelerated aging,* promoting in particular the COD effect. The advantage of using single current pulses is the chance to trigger the COD event and in this way to control and intentionally interrupt and stop it. Thus, the short pulses enable us to prepare early stages of degradation by applying a step-test scheme. This means that we start with a current I_0 below the actual value $I_{\rm COD}$, where COD occurs (*COD threshold*).

Manuscript received November 1, 2012; revised December 18, 2012; accepted December 19, 2012. Date of publication December 24, 2012; date of current version May 13, 2013.

M. Hempel, J. W. Tomm, and T. Elsaesser are with the Max-Born-Institut für Nichtlineare Optik und Kurzzeitspektroskopie, Max-Born-Straße 2A, Berlin 12489, Germany (e-mail: hempel@mbi-berlin.de; tomm@mbi-berlin.de; elsasser@mbi-berlin.de).

F. La Mattina, I. Shorubalko, and M. Stiefel are with the EMPA, Swiss Federal Laboratories for Materials Science and Technology, Dübendorf 8600, Switzerland (e-mail: Fabio.Lamattina@empa.ch; Ivan.Shorubalko@empa.ch; Michael.Stiefel@empa.ch).

I. Ratschinski, M. Schade, and H. S. Leipner are with the Interdisziplinäres Zentrum für Materialwissenschaften, Martin-Luther-Universität Halle-Wittenberg, Heinrich-Damerow-Straße 4, Halle/Saale 06120, Germany (e-mail: ingmar.ratschinski@cmat.uni-halle.de; martin.schade@cmat.uni-halle.de; hartmut.leipner@cmat.uni-halle.de).

F. M. Kießling is with the Leibniz Institut für Kristallzüchtung, Berlin 12489, Germany (e-mail: kiessling@ikz-berlin.de).

Color versions of one or more of the figures in this paper are available online at http://ieeexplore.ieee.org.

Digital Object Identifier 10.1109/JSTQE.2012.2236303

1077-260X/$31.00 © 2012 IEEE

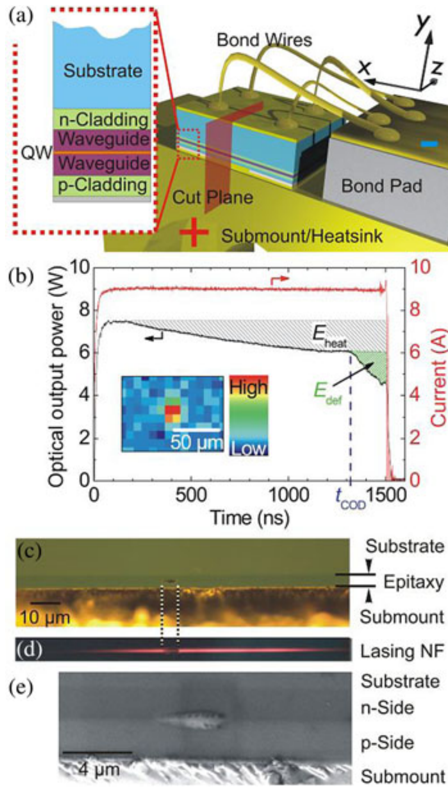

Fig. 1. (a) Scheme of the mounted diode laser. The orientation of the plane, where TEM cross sections have been cut is marked as a reddish *y–z* plane. The inset shows the epitaxial layer sequence. (b) Oscilloscope traces of the diode current and optical output power of device A, during the particular pulse in which COD took place. The energy missing in the optical output power (E_{def}) is shaded; it is the difference to the extrapolated curve without COD. The time t_{COD} is indicated. (c) Optical micrograph from the front facet of device A after COD. The bulged part of the defect is visible as a spot in the epitaxial layer. (d) Lasing near-field of the damaged laser taken at the same position as (c), but without external illumination and $I = 0.5$ A. (e) SEM image of the same defect as shown in (c) and (d).

Then a single current pulse of duration t_{pulse} is applied to the diode laser and the status of the device is monitored by recording the optical output power by a fast photodiode. Additionally, the front facet is monitored by a thermocamera, integrating over the entire laser current pulse length t_{pulse}. This helps us to detect the COD since it is related to a flash of Planck's radiation; Fig. 1(b) gives an example; see also [14]. If no sign of COD is detected, the current for the following step is increased by ΔI. Earlier we found a relationship between the current I_{COD} and the time t_{COD} (time between leading pulse edge and the moment where COD starts) [14]. By carefully approaching this point by choosing a constant short t_{pulse} and small ΔI-values, it becomes possible to prepare early stages of defect creation, because the one and only energy source of the COD process, the laser light, is switched off at the end of the pulse.

Utilizing this strategy, we prepared a set of 34 samples. In the following, we will focus on two devices named A and B. Device A experienced COD at $I_{\mathrm{COD}} = 9$ A with $t_{\mathrm{pulse}} = 1500$ ns, and $t_{\mathrm{COD}} = 1320$ ns. This gives a time of ∼180 ns for the defect to develop. The minimum energy for defect growth provided by the laser light was E_{def} ∼155 nJ, which is the difference of the output power between an extrapolated curve for the case of no COD occurrence and the real curve influenced by COD; see the shaded area in Fig. 1(b). Device B experienced an initial COD ignition at $I_{\mathrm{COD}} = 10$ A with $t_{\mathrm{pulse}} = 300$ ns, and $t_{\mathrm{COD}} = 225$ ns, incorporating an energy of 45 nJ. Thereafter, the defect growth was revived by a second 10-A pulse of 300 ns length providing 246 nJ of energy.

B. Preparation and Microscopy

The microscope systems and operation parameters which are used in this study are as follows: For transmission electron microscopy (TEM) investigations in diffraction contrast, a JEM 4000 FX was used at an acceleration voltage of 200 kV. To provide an overview of the defects, bright field images in multiple-beam orientation were recorded. The high-resolution TEM investigations were carried out using a JEM 4010 TEM at an acceleration voltage of 400 kV. Energy dispersive X-ray spectroscopy (EDX) was performed on a JEM 2200FS operating at 200 kV in scanning TEM mode. High-resolution images were taken by means of an ORION helium ion microscope from Carl Zeiss (henceforth referred to as "He-microscope"). The microscope is based on a He focused ion beam (FIB) that excites secondary electrons in the sample which are then detected. We operate it with a beam current of 0.5 pA at 30 kV.

To allow defect inspection, the devices have been prepared in cross section by means of a FEI *Strata* 235 Dual Beam Ga-FIB. This system consists of a scanning electron microscope (SEM) operating at a maximum of 30 kV and a Ga-FIB operating at 30 kV. The two columns are combined in a cross angle of 52°. The SEM allows for non-destructive inspection during the FIB cut.

Fig. 1(c) shows the COD signature at the front facet of device A as seen through an optical microscope with a 100× objective. The region marked as "epitaxy" contains the QW, cladding, and waveguide layers; see inset of Fig. 1(a). The location of the defect is also visible as distinct gap in the lasing near-field at $I = 0.5$ A; see Fig. 1(d). It is taken at exactly the same position as (c), as indicated by the dotted lines. A SEM image of the external front facet defect from the same device as in (c) and (d) is given in Fig. 1(e). SEM images clearly identify this structure as material extrusion. The labeling of the visible layers is in accordance with the inset of Fig. 1(a) and (c). In contrast to the optical micrograph in (c), the *n*- and *p*-doped sides may be distinguished in the SEM image, while no contrast is observed between the waveguide and the cladding. Furthermore, small dark features on both sides, top and bottom, of the extrusion are visible.

III. Results and Discussion

A. Microscopy of COD Pattern Generated in One Single Pulse

We now discuss the analysis of device A by high-resolution microscopy. All FIB cuts are oriented perpendicular to the QW plane along the resonator axis in the *y–z* plane, as indicated by the reddish plane in Fig. 1(a). Fig. 2(a) gives an overview image taken with the He-microscope from a cross section, which was

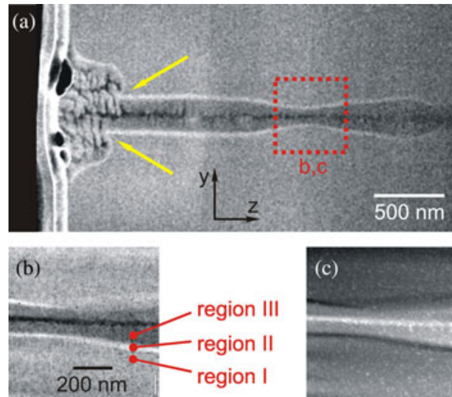

Fig. 2. (a) Cross section He-microscope image of device A in the y–z plane. The abrupt contrast change about 1.3 μm right from the front facet along z is a result of earlier imaging. Features that are highlighted by the yellow arrows are discussed in the text. (b) and (c) TEM images of the part of the cross section marked by the dotted red line in (a), in (b) bright-field contrast mode is used, while dark-field contrast mode is used in (c).

obtained by a cut through the center of the particular defect, which is precharacterized by the results shown in Fig. 1(b)–(e). Under the front facet coating, one clearly sees holes. During the FIB preparation of the samples, it became clear that these hollow spaces are identical with the dark features visible in SEM images of the external damage around the center of the damage site, but never on top of the QWs; see also Fig. 1(e). The defect beneath the surface consists of modified material surrounded by a thin sharp line appearing bright in the used contrast mode. Therefore, we will refer to this phenomenon as *white line*, even if its gray value depends only on the used measurement mode. After the inspection by He-microscopy, a ∼100-nm thick TEM lamella is prepared by applying an additional FIB cut from the opposite side. Fig. 2(b) and (c) show the region on an expanded scale, which is indicated by a square in Fig. 2(a). They are obtained in elastic scattering TEM mode with a bright-field detector (b) and inelastic scattering mode with a high-annular dark-field detector (c). The contrast inversion between both images, also known as *chemical contrast*, proves the presence of different element concentrations. In order to analyze this, an EDX measurement is performed at the regions indicated in Fig. 2(b). The region denoted as “I” represents the material outside the damage, “II” is directly at the *white line*, and “III” is between the former QW position and the *white line* surrounding the defect. The resulting EDX spectra are shown in Fig. 3(a); the respective transitions and elements are given at the peaks. Fig. 3(b)–(d) summarizes the change in the element concentrations normalized to the outer region I. The same result is obtained by selecting equivalent measurement points at the opposite side, in y-direction, of the former QW.

B. Analysis of COD Pattern Generated in Two Consecutive Single Pulses

After analyzing the defect created by a single pulse, the question that arises is: What happens in the case of applying a second current pulse and provoking further damage? Such a *COD reignition* by the application of further single pulses has been

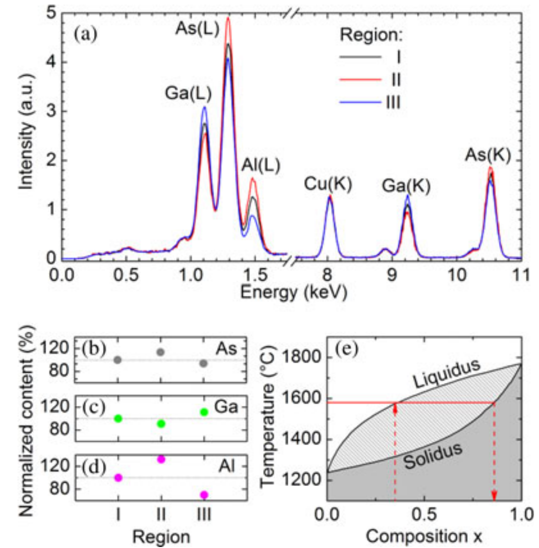

Fig. 3. (a) EDX analysis at the three regions indicated in Fig. 2(b), the elements and respective core-shells are labeled. (b)–(d) The relative changes of element content normalized to region “I” are given for As (b), Ga (c), and Al (d). The data are taken from the EDX measurements in (a). (e) Pseudobinary $Al_{1-x}Ga_xAs$ phase diagram, data taken from [21]. The line at 1580 °C and the arrows have been discussed in the text.

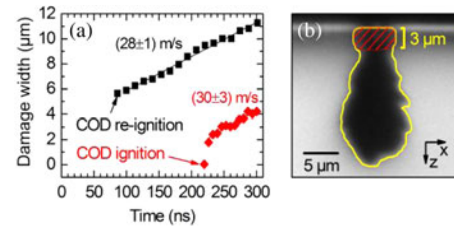

Fig. 4. Temporal evolution of the damage width (extension in x-direction) during the pulse where COD occurs and during the successive one where COD reignites, data from [2]. The lateral velocities of the damage propagation are determined by linear fitting of the data points. (b) Micro photoluminescence map of the QW (in the x–z plane) near the front facet (at the top of the image). The area surrounded by the yellow line gives the area of the damage pattern after both pulses; the red-shaded area indicates the estimate for the area after the first COD ignition.

used earlier as a technique for time-slicing the COD-related defect propagation [13], [15]–[17]. Before analyzing the resulting damage pattern at the location, where the process gets continued, e.g., by TEM, it is important to know exactly, where the reignition actually took place. This was determined as follows.

The damage extension within the initial single pulse (that leads to COD) in the x-direction inside the laser is measured *in-situ*. This is done by streak camera measurements of the lasing near-field [17]. The identification of the width of the region of reduced near-field with the internal defect width was verified in [17] and [18]. Results for the first pulse and the successive one are shown in Fig. 4(a). The velocity of the damage extension during the two pulses keeps almost constant, as indicated by the linear fits in concert with the resulting slopes; see Fig. 4(a). This indicates homogeneous defect growth. Therefore, we assume that the shape of the damage pattern can be scaled linearly. Between the application of the two current pulses resulting in the two COD events and the TEM preparation of the device a

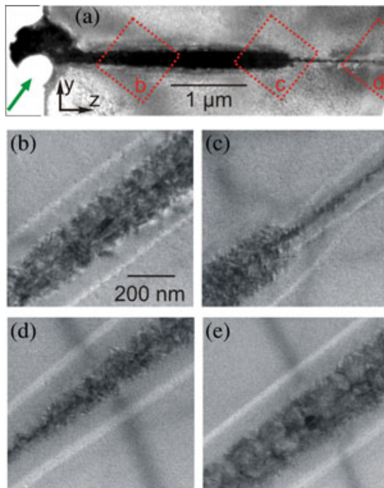

Fig. 5. Results obtained from the analysis of device B: (a) TEM overview image of the front part of the cross section in y–z plane. The arrow points to the hollow space under the front facet coating. (b)–(e) TEM images on an enlarged scale taken at the positions marked in (a) and in the case of (e) from a position right of "d" in (a).

micro-photoluminescence map of the QW emission was taken; see Fig. 4(b). The dark area indicates the material being severely damaged. As shown in the preceding section, the thickness of the defect (in y-direction) can be considered constant, except for the region close to the facet. Therefore, the scaling of the volume damage is restricted to scaling of the damaged area; see Fig. 4(b). The final area of the damage, including both COD events is $A_{\mathrm{final}} = 139\ \mu\mathrm{m}^2$; see the yellow line in Fig. 4(b). We now linearly scale this area from the width of 11.3 μm along the x-direction of the final damage pattern to the 4.2 μm after the first pulse, as obtained from Fig. 4(a), while keeping the aspect ratio constant. We end up with an area of 23 $\mu\mathrm{m}^2$ for the damage after the first pulse. Following our investigations about COD-related defect growth [13], [19], it is valid to reshape the area slightly while keeping the area and its x-extension constant. The area assumed to be affected by the first COD event is red-shaded in Fig. 4(b). Now its dimension along the resonator axis z can be estimated. A value of $\sim$3 μm is found.

We prepared device B in a way that this particular location was available for TEM analysis. A $\sim$200-nm thick lamella was cut in a y–z plane right out of the middle of the extrusion that tops the defective region at the facet. The cross section is investigated by the JEM 4000 FX and the JEM 4010 microscopes. While Fig. 5(a) gives an overview, Fig. 5(b)–(e) presents the details of the damage pattern in the vicinity of the former QW plane. The positions where images (b)–(d) were taken are highlighted by dotted rectangles in (a). Fig. 5(e) is located right from (d) along the QW. The region around the front facet is visible in Fig. 5(a). Here a hollow space, see arrow, as seen in Fig. 2, is also visible under the coating, which has been removed during preparation from this sample.

As in the He-microscope investigation, cf., Fig. 2, a *white line* surrounds the entire damaged region. While the thickness of the defect is nearly constant in (b) and (e), it is substantially reduced in (c). At this particular location, namely at $z\sim3$ μm, we observe the damage pattern becoming abruptly thinner. In addition, we find *two closely separated white lines* for the one and only time on each side of the defect.

Therefore, we consider it highly likely that Fig. 5(c) indeed shows the location, where the COD reignition took place.

C. Nature of the White Line

Some earlier papers [8]–[11], [20] have revealed a similar *white line*, as visible in Figs. 2 and 5, by TEM analysis of the defect pattern. In contrast to this study, they investigated devices emitting at 980 nm and used TEM lamellas cut perpendicular to the light direction in the x–y plane (except for [10]). These reports focus on the diffusion of In (from their In-rich QWs) during gradual degradation and COD, without directly claiming, e.g., the cause of the *white line* to be due to In enrichment. Since thickness and contrast of the *white line* including the sharp bends are almost uniform throughout all images, diffusion processes starting at the QW are considered extremely unlikely causes. The lack of In in our 808-nm emitting device structure fully eliminates this explanation for the devices investigated here.

We interpret the *white line* as a recrystallization front that gets formed after melting of the $\mathrm{Al_{0.35}Ga_{0.65}As}$ waveguide. The line of arguments is as follows: EDX and *chemical contrast* analysis show the *white line* to represent regions with reduced Ga and increased Al and As content; see Fig. 3(a)–(d). In order to rule out, that the concentration change measured by EDX come from graded regions in the pristine material, additional measurements were made at comparably located, but undamaged sites. Here absolutely no composition change was detected within the error limits.

The energy freed during damage creation, see Section III-D, causes temperatures high enough to melt $\mathrm{Al}_x\mathrm{Ga}_{1-x}\mathrm{As}$ of any composition. The necessary melt temperatures can be obtained from the phase diagram of the Al–Ga–As system or from the pseudobinary GaAs–AlAs part [21], see Fig. 3(e). The system obeys no miscibility gap, and any composition can be obtained. The minimum temperature at which the material is liquid can be taken from the liquidus area of the phase diagram. Assuming that a certain volume of material was molten, the inverse process—namely solidification—is of interest. Initially, the melt is expected to have the same composition as the surrounding solid material, namely $\mathrm{Al_{0.35}Ga_{0.65}As}$. Segregation effects, however, cause the solidification process not to result in material with uniform composition. The compositions can be calculated from liquidus and solidus in the phase diagram and are expressed by the ratio of the mole fraction in the solid to the mole fraction in the melt. This segregation coefficient k is not constant and varies in dependence on the composition. Looking at the pseudobinary phase diagram $k > 1$, or in other words Al-rich solid solutions are in equilibrium with the Ga-rich melts. These composition values can easily be estimated from the tie lines, which connect liquidus and solidus at a given temperature. Starting, e.g., with a melt composition of $(\mathrm{GaAs})_{0.65}(\mathrm{AlAs})_{0.35}$, i.e., at $\sim$1580 °C and taking $k\sim2.4$, the composition which is in equilibrium with this melt and solidifies first, is roughly $(\mathrm{GaAs})_{0.17}(\mathrm{AlAs})_{0.83}$, see lines in Fig. 3(e). As a result of this process, the remaining

melt becomes depleted in Al. As the cooling process continues, the liquidus temperature decreases due to its Al-depletion. Consequently, the Al-content in the composition of the solid solution is also reduced. Assuming the solidification process to be core-directed, an Al-rich solid solution should be found adjacent to the surrounding matrix. This is exactly what we see as the *white line*. As the solidification continues, the Al-content decreases continuously.

Furthermore, one has to keep in mind the described process to be only valid for equilibrium conditions. Assuming equilibrium for the very first incremental volume element solidified, the conditions for the following crystallization might change dramatically. Looking at Fig. 2(a) again, we find a rough answer to these solidification parameters. After crystallization of some Al-rich material forming the *white line,* the growth becomes morphologically unstable and dendrites are observed, which grew due to constitutional supercooling. Dendrites are a clear hint of non-equilibrium growth conditions due to violations of interface stability limits [22]. After solidification one has certainly to take into account diffusion at these temperatures but it seems not to change significantly the measured concentration profile. Thus, recrystallization can qualitatively explain the genesis of the Al-rich *white line,* which therefore represents something like an *isothermal line* illustrating the recrystallization front.

D. *Energy Involved in Damage Creation*

An advantage of the step-test approach is the knowledge about the energy feeding damage growth. We claimed that the shaded area in Fig. 1(b) represents this damage energy E_{def}. It is the difference between a hypothetical curve for the pulse without COD $P_{\text{hypo}}(t)$ and the actual measured one $P_{\text{real}}(t)$ for the time span between COD occurrence at t_{COD} and the pulse end t_{end}. The curve for the COD-free case is obtained by scaling the curve from the previous current step.

To assess the mechanisms of a power decrease other than reabsorption in the material, the small amount of optical power transmitted through the high-reflecting rear facet was analyzed. This power displays minor changes at times longer than t_{COD} (cf., Fig. 1(b)), pointing to minor changes of the total optical intracavity power of the device. We, thus, conclude that the drop of output power at the front facet (see Fig. 1(b), $t > t_{\text{COD}}$) allows for a realistic estimate of the damage energy E_{def}.

The damage energy is calculated as

$$E_{\text{def}} = \int_{t_{\text{COD}}}^{t_{\text{end}}} [P_{\text{hypo}}(t) - P_{\text{real}}(t)]\text{d}t. \tag{1}$$

The corresponding area is green-shaded in Fig. 1(b). The value obtained is $E_{\text{def}} = 155$ nJ.

One might ask if it is also necessary to consider the reabsorbed light energy E_{heat} which heats up the bulk. In order to estimate an upper limit for E_{heat}, we can consider it to be the drop in optical output power during the single pulse. To calculate the value of E_{heat} we have to integrate the area between a constant curve set to the maximal power obtained at the beginning of the pulse at $t_{\max}$ (in Fig. 1(b) at ~150 ns) and $P_{\text{hypo}}(t)$:

$$E_{\text{heat}} = \int_{t_{\max}}^{t_{\text{end}}} [P_{\max} - P_{\text{hypo}}(t)]\text{d}t. \tag{2}$$

The corresponding area is gray-shaded in Fig. 1(b). The obtained value is $E_{\text{heat}} = 1337$ nJ. This value is ten times larger than the one for E_{def}; cf., the ratio between the shaded areas.

The volumes where these energies are freed differ much more. The energy E_{heat} is absorbed in the entire emitter stripe with the volume V_{emitter} = length × width × thickness = 1.4 mm × 50 μm × 1 μm = $7{\times}10^4$ μm^3. The thickness value of 1 μm corresponds to the waveguide thickness. The damage volume is taken as the one being surrounded by the *white line*, namely $V_{\text{def}} \sim 2.4$ μm^3. Taking into account the different volumes, we can estimate the corresponding energy densities for bulk heating (assuming a homogeneous distribution, even if it is known that the temperature is slightly higher around the front facet) w_{heat} = 19 pJ/μm^3, and for the damaged volume w_{def} = 65 nJ/μm^3. They differ by more than three orders of magnitude. This verifies the assumption that the contribution of E_{heat} can be neglected while dealing with the damage growth. Notice that the contribution of E_{heat} is nevertheless important for reaching the so-called critical temperature; see [1] that is needed to start COD and subsequent damage growth.

Keeping the energies and the volumes in mind, we estimate the temperature rise in the material. Caused by the short pulse time and the even shorter time between t_{COD} and t_{end}, it is valid to neglect the heat transport in the device. Therefore, we can use the following simple expression:

$$E = c \cdot \rho \cdot V \cdot \Delta T \Rightarrow \Delta T = \frac{E}{c \cdot \rho \cdot V} \tag{3}$$

with the material parameters for $\text{Al}_{0.35}\text{Ga}_{0.65}\text{As}$, namely specific heat $c = 0.372$ J/(g K) and the mass density $\rho = 4.77$ g/cm^3. Putting in the values of E_{heat} and V_{emitter} for the bulk heating, we end up with ΔT_{bulk} ~11 K. This value is approximately half the temperature rise expected from a measurement of spectral shift of the emission line [17]. The measurement itself was done by using a grating monochromator equipped with an intensified CCD camera. Gating the intensifier allows for effective integration times of 10 ns. This integration window was shifted along the 1-μs pulse. The repetition rate was 1 Hz.

This is an effect of the averaging over the entire volume. However, since both values are on the same order of magnitude, the assumptions we made are right.

The same analysis using (3) can now be made with the data obtained for the damaged volume. Using V_{def} and E_{def} we get ΔT ~$3.6{\times}10^4$ K. This value is much too high because the melting temperature for $\text{Al}_{0.35}\text{Ga}_{0.65}\text{As}$ is T_{melt}~1580 °C. Here, two questions arise: Is the statement that the bulk heating can be neglected when discussing the damage growth still valid, and what does this high value mean?

We start with the first. Taking into account the energy E_{def} and calculating the volume, by using (3), that can be heated to T_{melt} we get a value of ~80 μm^3 which is still three orders of magnitude smaller than V_{emitter}, suggesting that bulk heating plays a minor role.

The second question on the high temperature estimate leads us directly back to the nature of the *white line*. Taking into account energy calculations presented in the past [14], [17] it is highly likely that the assumption that the *white line* represents the border of the damaged region is incorrect. Investigations of point defect distributions in conjunction with time-resolved thermography indicate that the heat is distributed across a substantially larger volume and still creates point defects there [13]. Thus, the area outside the *white line* is not undamaged and the *white line* is rather the border around the most severely damaged material fraction, i.e., represents an *isothermal line within the damaged material*.

E. Sequence of Events

Inside the cavity, the *white lines* follow the QW with almost fixed spacing, which implies a constant temperature during defect propagation within a single pulse. Moreover, the distance of the *white line* on the p- and n-side from the location, where the QW has been, is the same. This clearly indicates the QW as origin of the propagating defect.

In vicinity of the front facet, however, the situation is different. Here, the obviously damaged region has a substantially larger extent in y-direction. Nevertheless, the *white line* maintains its sharp shape. The specific line shape with the characteristic corners, marked by yellow arrows in Fig. 2(a), indicates the existence of separate initial points of COD on both sides of the QW. One single starting point at the QW position could definitely not explain a temperature distribution represented by the isothermal line including corners. Defect patterns showing such inhomogeneous structures were also reported for single-spatial-mode-lasers failed during long-term degradation in "kink-free"[1] operation [10]. This finding is very important for our line of arguments, since it rules out the possibility that our results are an effect of higher order spatial modes[2] emerging at elevated currents (as used in our methodology). This once again also justifies the use of the step-test approach for COD analysis. Additional evidence for separate starting points is given by the positions of the hollow spaces under the coating that have been originally discovered by looking at the front facet before device preparation; see Fig. 1(e). They are always located on top of the waveguide next to the QW plane, but never on top of the QW itself.

We propose the most likely scenario to be as follows: Fast, nearly isotropic (in the y–z plane) damage spread starts in the *waveguide* close to the front facet, affecting soon the QW. Now, all further defect growth takes place along the QW itself. This is plausible, because the highest light field intensity is expected there. After defects make a portion of the QW absorptive, this location will be the starting point for further damage propagation within the QW plane.

In the case of device B, where we applied two consecutive high current single pulses, we find an *overlap of the two thermo-cycles*, without the presence of any additional extended damage pattern as observed at the facet.

The evaluation of thermal images for successive single pulses, however, show no significant differences in the magnitudes of the thermal signals taken for the initial and second COD ignition; see also [13], [15], [16]. This points to temperatures being on the same order. A constant temperature during the damage propagation process also explains why constant defect growth velocities were found in the past [13], [16], [23].

Therefore, the mechanisms starting the defect growth during the initial and second COD ignition must be very different.

1) An *explosion-like first COD ignition* at the laser facet, which has its origin rather at the waveguide than at the QW.
2) A *COD reignition* in the defect path around the severely damaged plane, where the QW has been located before. There is a local overlap of the end of the first defect growth step and the beginning of the successive one. The width (in y-direction) of the damage is locally distorted, but retrieves its former extent within $<2\ \mu$m. In sharp contrast to the first ignition, the *white line* indicates here a rather smooth restart.

This makes the first COD ignition a unique event. Its physical background and the one of the reignition in the subsequent pulse are different, calling for more detailed investigations.

IV. Conclusion

We have demonstrated the preparation of extremely early phases of defect growth during COD and their microscopic investigation. We identify a clear difference between the defect pattern generated by the initial COD event at the front facet and the COD reignition site. In the case of the initial starting point, we find strong evidence that the waveguide on both sides of the QW has a major influence on the start of the COD process. Furthermore, we have justified the former proposed methodology of time slicing the COD process by successive short pulses. The appearance of the locations, where the process is revived, is found to differ only slightly from a region, where regular defect propagation took place. Although COD reignition involves the same high temperatures as the initial COD-event, the corresponding damage sites are rather unremarkable. Defect propagation and reignition are driven by processes being originated at the QW. Our findings regarding COD reignition can probably be extended to COD events taking place in the bulk (catastrophic optical bulk damage). The microscopic analysis emphasizes the uniqueness of the initial COD event and points the attention of future research to the waveguides close to the front facet.

Acknowledgment

The authors would like to thank P. Werner, Max-Planck-Institut für Mikrostrukturphysik Halle, for the support of the TEM investigations and the SNSF R'equip (206021_133823) for the possibility to use the new He–Ion microscope at EMPA.

[1]The term "kink-free" stands here for an operation regime, where the device indeed works in single-spatial-mode operation without the presence of any higher order spatial modes.

[2]Higher order spatial modes are expected to have peak intensities in the waveguide part of the facet.

REFERENCES

[1] J. W. Tomm, M. Ziegler, M. Hempel, and T. Elsaesser, "Mechanisms and fast kinetics of the catastrophic optical damage (COD) in GaAs-based diode lasers," *Laser Photonics Rev.*, vol. 5, no. 3, pp. 422–441, 2011.

[2] C. Harder, "Pump diode lasers," in *Optical Fiber Telecommunications V A Components and Subsystems*, I. P. Kaminov, T. Li, and A. E. Willner, Eds. Amsterdam, The Netherlands: Elsevier, 2008, pp. 107–122.

[3] T. Kamejima and H. Yonezu, "Catastrophic optical damage generation mechanism in (AlGa)As DH lasers," *Jpn. J. Appl. Phys.*, vol. 19, pp. 425–429, 1980.

[4] S. Mahajan, H. Temkin, and R.A. Logan, "Formation of optically induced catastrophic degradation lines in InGaAsP epilayers," *Appl. Phys. Lett.*, vol. 44, no. 1, pp. 119–121, 1984.

[5] S. N. G. Chu, S. Nakahara, M. E. Twigg, L. A. Koszi, E. J. Flynn, A. K. Chin, B. P. Segner, and W. D. Johnston, "Defect mechanisms in degradation of 1.3-μm wavelength channeled-substrate buried heterostructure lasers," *J. Appl. Phys.*, vol. 63, no. 3, pp. 611–623, 1988.

[6] O. Ueda, K. Wakao, S. Komiya, A. Yamaguchi, S. Isozumi, and I. Umebu, "Catastrophic degradation of InGaAsP/InGaP double-heterostructure lasers grown on (001) GaAs substrates by liquid-phase epitaxy," *J. Appl. Phys.*, vol. 58, no. 11, pp. 3996–4002, 1985.

[7] C. W. Snyder, J. W. Lee, R. Hull, and R. A. Logan, "Catastrophic degradation lines at the facet of InGaAsP/InP lasers investigated by transmission electron microscopy," *Appl. Phys. Lett.*, vol. 67, no. 4, pp. 488–490, 1995.

[8] I. Rechenberg, A. Hopner, J. Maege, A. Klein, G. Beister, and M. Weyers, "Heating and damage of InGaAs/GaAs/AlGaAs laser facets," in *Proc. Inst. Phys. Conf. Series Microsc. Semiconducting Mater.*, 1995, vol. 146, pp. 587–590.

[9] I. Rechenberg, U. Richter, A. Klein, W. Hoppner, J. Maege, and G. Beister, "Early stage of facet degradation in 980 nm pump laser diodes," in *Proc. Defect Recognit. Image Process. Semiconductors*, 1997–1998, vol. 160, pp. 479–482.

[10] Y. Sin, N. Presser, B. Foran, M. Mason, and S.C. Moss, "Investigation of catastrophic optical mirror damage in high power single-mode InGaAs-AlGaAs strained quantum well lasers with focused ion beam and HR-TEM techniques," in *Proc. Conf. Lasers Electro-Optics, 2007*, Baltimore, MD, 2007, pp. 1423–1424.

[11] Y. Sin, N. Presser, B. Foran, N. Ives, and S. C. Moss, "Catastrophic facet and bulk degradation in high power multi-mode InGaAs strained quantum well single emitters," *Proc. SPIE*, vol. 7198, pp. 719818-1–719818-12, 2009.

[12] http://www.intenseco.com/products/hpd/components/Series1000.asp, 2012.

[13] M. Hempel, F. La Mattina, J. W. Tomm, U. Zeimer, R. Broennimann, and T. Elsaesser, "Defect evolution during catastrophic optical damage of diode lasers," *Semicond. Sci. Technol.*, vol. 26, no. 7, p. 075020, 2011.

[14] M. Ziegler, M. Hempel, H. E. Larsen, J. W. Tomm, P. E. Andersen, S. Clausen, S. N. Elliott, and T. Elsaesser, "Physical limits of semiconductor laser operation: A time-resolved analysis of catastrophic optical damage," *Appl. Phys. Lett.*, vol. 97, no. 2, p. 021110, 2010.

[15] M. Hempel, M. Ziegler, J. W. Tomm, T. Elsaesser, N. Michel, and M. Krakowski, "Time-resolved analysis of catastrophic optical damage in 975 nm emitting diode lasers," *Appl. Phys. Lett.*, vol. 96, no. 25, p. 251105, 2010.

[16] M. Hempel, J. W. Tomm, M. Ziegler, T. Elsaesser, N. Michel, and M. Krakowski, "Catastrophic optical damage at front and rear facets of diode lasers," *Appl. Phys. Lett.*, vol. 97, no. 23, p. 231101, 2010.

[17] M. Hempel, J. W. Tomm, M. Baeumler, H. Konstanzer, J. Mukherjee, and T. Elsaesser, "Near-field dynamics of broad area diode laser at very high pump levels," *AIP Advances*, vol. 1, no. 4, p. 042148, 2011.

[18] M. Hempel, J. W. Tomm, M. Baeumler, H. Konstanzer, J. Mukherjee, and T. Elsaesser, "Near-field characteristics of broad area diode lasers during catastrophic optical damage failure," *Proc. SPIE*, vol. 8432, pp. 84320O-1–84320O-7, 2012.

[19] M. Hempel, J. W. Tomm, U. Zeimer, and T. Elsaesser, "Defect propagation in broad-area diode lasers," *Mater. Sci. Forum*, vol. 725, pp. 101–104, 2012.

[20] S. N. G. Chu, N. Chand, W. B. Joyce, P. Parayanthal, and D. P. Wilt, "Generic degradation mechanism for 980 nm InxGa1-xAs/GaAs strained quantum-well lasers," *Appl. Phys. Lett.*, vol. 78, no. 21, pp. 3166–3168, 2001.

[21] L. M. Foster, J. E. Scardefield, and J. F. Woods, "Thermodynamic analysis of the III–V alloy semiconductor phase diagrams," *J. Electrochem. Soc.*, vol. 119, no. 6, pp. 765–766, 1972.

[22] W. A. Tiller, "Theoretical analysis of requirements for crystal growth from solution," *J. Crystal Growth*, vol. 2, no. 2, pp. 69–79, 1968.

[23] J. H. Jacob, R. Petr, M. A. Jaspan, S. D. Swartz, M. T. Knapczyk, and A. M. Flusberg, "Fault protection of broad-area laser diodes," *Proc. SPIE*, vol. 7198, p. 719815, 2009.

Martin Hempel received the diploma in physics from the Humboldt University, Berlin, Germany, in 2009, where the topic of his thesis was quantum cascade lasers. He is currently working toward the Ph.D. degree at Max Born Institute, Berlin, Germany, focusing on optoelectronic devices and especially on the COD effect.

Mr. Hempel is a member of the Deutsche Physikalische Gesellschaft, Germany.

Jens W. Tomm received the Diploma and the Ph.D. degree in physics from the Humboldt University, Berlin, Germany.

From 1993 to 1995, he was with the Georgia Institute of Technology, Atlanta, and in 1999 he was with Riken, Sendai, Japan. In 1995, he became a member of the scientific staff of the newly founded Max Born Institute, Berlin, Germany, where he currently runs the "Optoelectronic Device" group. His research interests include photonics, optoelectronics, and semiconductor physics. He has organized international conferences, edited conference proceedings, and authored more than 240 peer-reviewed papers, three reviews, six patents, and one book.

Dr. Tomm is a member of the German Physical Society, the E-MRS, and the Optical Society of America.

Fabio La Mattina received the Diploma degree from the Physics Institut, Univerisy of Palermo, Palermo, Italy, in 2004, and the Ph.D. degree from the Physics Intitut, University of Zurich, Switzerland, in 2008. From 2005 to 2008 he performed part of his Ph.D. work at the IBM Zurich Research Lab in the research staff of Storage & Memory Technology in the project of "Resistance change memory."

Since 2008, he has been a Scientist in the laboratory of Micro- and Nano-electronics/Metrology/Reliability at EMPA, Dübendorf, Switzerland.

Ingmar Ratschinski received the diploma in physics from the Martin-Luther-Universität Halle-Wittenberg, Halle, Germany, in 2008 where the topic of his thesis was materials physics. He is currently working toward the Ph.D. degree at the Interdisziplinäres Zentrum für Materialwissenschaften, Halle, where his thesis is about indentation-induced dislocations and cracks in GaN and GaAs.

His research interests include microscopy (SEM, TEM, AFM) and semiconductor physics (GaN, GaAs).

Mr. Ratschinski is a member of the Deutsche Physikalische Gesellschaft, Germany.

Martin Schade received the diploma in physics from the Martin-Luther-Universität Halle-Wittenberg, Halle, Germany, in 2007, where the topic of his thesis was in physics. He is currently working toward the Ph.D. degree at the Interdisziplinäres Zentrum für Materialwissenschaften, Halle, where his thesis is about analytical transmission electron microscopy of nanostructures containing silicon polymorphs.

His research interests include electron microscopy and spectroscopy (HRTEM, EELS, Raman) as well as silicon-based physics.

Mr. Schade is a member of the Deutsche Physikalische Gesellschaft, Germany.

Ivan Shorubalko received the Ph.D. degree in physics from Lund University, Lund, Sweden. The focus of his reasearch was on electrical properties of quantum and ballistic nanodevices fabricated from III–V semiconductors.

He was also a Postdoctoral Researcher in the nanophysics group at ETH Zurich, Switzerland, where he was involved inconducting research on designing and manipulating electron quantum states in semiconductor nanostructures based on InAs nanowires. He joined Electronics/Metrology/Reliability lab at EMPA, Duebendorf, Switzerland as a Scientist in 2009. His research interests include graphene-based nanoelectronic devices functioning at room temperature, plasmonics, nano-optics, and a wide range of nanofabrication techniques. He has authored more than 60 peer-reviewed papers.

Michael Stiefel is a Microscopist at EMPA, Duebendorf, Switzerland. He is currently studying material and process engineering at the Zurich University of Applied Science, Winterthur, Switzerland.

His research activities are focused on electron and ion beam microscopy for semiconductor and material science applications.

Hartmut S. Leipner received the Diploma in physics from Charles University, Prague, Czechoslovakia, in 1982. He received the Dr. rer. nat. degree and the Dr. habil. degree in physics, both from Martin Luther University Halle-Wittenberg, Halle, Germany in 1987 and 2002, respectively.

He joined the Interdisciplinary Center of Materials Science, Halle, in 2005 as the Chief Science Officer. His research interest concentrates on electron-microscopy-based high-resolution analysis, together with other characterization tools—such as positron annihilation or optical spectroscopy—and the development of new nanostructuring methods in the field of materials for renewable energies. He has been continuously interested in the investigation of the character of structural defects, their formation and dynamics, and the interaction of different types of defects in semiconductor devices.

Dr. Leipner is member of the Executive Board of the German Physical Society and the Chairman of the Microanalysis Division. He is member of the IUPAP C10 commission on solid-state physics, the Materials Research Society, and the German Thermoelectric Society.

Frank M. Kießling was born in Altdöbern, Germany, in 1960. He received the Diploma and the Dr. rer. nat. degree in crystallography, both from the Humboldt University of Berlin, Germany, in 1986 and 1991, respectively.

He joined the CEA-Saclay, National Institute for Nuclear Science and Technology, Gif-sur-Yvette, France, as a Postdoctoral Fellow in 1991, dealing with positron annihilation of II–VI and III–V compounds. From 1994 to 1996, he was a Visiting Scholar where his area of interest was in the growth and analysis of I–III–VI2 nonlinear optical materials at Stanford University, Center for Materials Research, Stanford, CA. His principal research interests include both crystal growth by various methods and defect analysis of semiconductor materials. Since 2001, he has been a Senior Researcher at the Leibniz Institute for Crystal Growth, Berlin, Germany, and is now heading the multi-crystalline Silicon group.

Dr. Kießling is a member of the Deutsche Gesellschaft für Kristallzüchtung und Kristallwachstum e. V.

Thomas Elsaesser received the Dr. rer. nat. degree in physics from the Technical University, Munich, Germany, in 1986. After working as a Research Associate and spending a postdoctoral period at AT&T Bell Laboratories, Holmdel, NJ, he finished his habilitation at the Technical University, Munich, in 1991.

Since 1993, he has been a Director of the Max-Born-Institut, Berlin, Germany, holding a joint appointment with Humboldt University, Berlin. He has contributed to a broad range of research in ultrafast science with processes in condensed matter representing the main area of his scientific work. He applies methods of both ultrafast optics and x-ray science. His major topics are transient structures as well as basic microscopic interactions and nonequilibrium dynamics in (bio)molecular systems and in solids, in particular semiconductors. He has authored more than 400 publications and holds six patents.

Dr. Elsaesser is a Fellow of the American Physical Society and the Optical Society of America.